Rodríguez-Laguna, J., Ibáñez Berganza, M. y Sierra, G. (2014). Energy space entanglement spectrum of pairing models with s-wave and p-wave symmetry. *Physical Review B*, 90(4), 041103(R).

DOI: https://doi.org/10.1103/PhysRevB.90.041103

PHYSICAL REVIEW B **90**, 041103(R) (2014)

Energy space entanglement spectrum of pairing models with s-wave and p-wave symmetry

Javier Rodríguez-Laguna
Mathematics Department, Universidad Carlos III de Madrid, Spain and Institute of Photonic Sciences (ICFO), Barcelona, Spain

Miguel Ibáñez Berganza
Istituto per i Processi Chimico-Fisici (CNR) and Dipartimento di Fisica, Università "La Sapienza", Roma, Italy

Germán Sierra
Instituto de Física Teórica (IFT), UAM-CSIC, Madrid, Spain

(Received 5 August 2013; revised manuscript received 21 June 2014; published 11 July 2014)

We study the entanglement between blocks of energy levels in 1D models for s-wave and p-wave superconductivity. The ground state entanglement entropy and entanglement spectrum (ES) of a block of ℓ levels around the Fermi point is obtained and related to its physical properties. In the superconducting phase at large coupling, the maximal entropy grows with the number of levels L as $\frac{1}{2}\ln(L)$. The number of levels presenting maximal entanglement is shown to estimate the number of Cooper pairs involved in pairing correlations. Moreover, the properties of the ES signal the presence of the Read-Green quantum phase transition in the $p+ip$ model, and of the Moore-Read line, which is difficult to characterize. This work establishes a link between physical properties of superconducting phases and quantum entanglement.

DOI: 10.1103/PhysRevB.90.041103 PACS number(s): 74.20.Fg, 03.67.−a, 05.30.Rt, 74.20.Rp

Introduction. The concept of entanglement entropy has proved to be extremely useful to characterize quantum phase transitions in many-body systems [1]. However, a deeper understanding can be achieved in terms of the entanglement spectrum [2], which in two-dimensional systems underlies the bulk-edge correspondence [3]. For example, it has been reported to distinguish between topologically different phases [4]. Most studies of the entanglement properties are performed in real space, but some physical systems are formulated naturally in momentum or energy space. Important examples are the models of superconductivity, where the Hilbert space is based on single-particle energy levels. In that spirit, the concurrence between modes in BCS systems was studied in the grand-canonical [5] and the canonical ensembles [6]. Entanglement between regions in Fourier space has been studied in [7]. The application of the density matrix renormalization group (DMRG) in momentum space [8] suggests that entanglement in Fourier space might be significantly lower than in real space for some problems.

In this work we study the entanglement entropy (EE) and entanglement spectrum (ES) of the ground state of the BCS Hamiltonians with s-wave and p-wave symmetry in the canonical ensemble. The s-wave Hamiltonian has been extensively used to describe the superconducting properties of ultrasmall metallic grains [9,10]. Several numerical studies found that, when the size of the grains is reduced, the BCS superconducting regime makes a smooth crossover to a fluctuation-dominated regime. Here we characterize the two regimes, and the transition between them, analyzing the EE and ES of the ground state. The $p+ip$-wave model of superconductivity has recently received a lot of attention due to its connection with the fractional quantum Hall effect at filling fraction 5/2 [11], and the possibility of experimental realization is undergoing very active research [12]. The model considered here is 1D, but it shares with its 2D counterpart a rich phase diagram that consists of three regions separated by a third-order and a zero-order transition line [13,14]. Again, we characterize these transitions using the ES. The analysis of these two models has been done using the DMRG method extending the previous results of Ref. [15]. The study of the topological phase transition in p-wave superconductors via the ES in real space was pioneered in [16]. In contrast, we perform our study in energy space.

s-wave model. The BCS Hamiltonian with s-wave symmetry is given by [9]

$$H_s = \sum_{j=1}^{L} 2jd\, b_j^\dagger b_j - gd \sum_{j\neq j'}^{L} b_j^\dagger b_{j'}, \tag{1}$$

where $i,j = 1,\ldots,L$ label single-particle energy levels, with energies jd, d is the level spacing, g is the dimensionless BCS coupling constant, and b_j ($b_j^\dagger$) are annihilation (creation) operators of fermions in time-reversed pairs, that is, hard-core boson operators. Richardson showed that (1) is exactly solvable by the Bethe ansatz [17], and Gaudin proved that in the large-N limit, the ground state energy and excitations coincide with those obtained with the grand-canonical BCS wave function [18]. The DMRG method was applied successfully to (1), reproducing the exact results [15].

The physics described by the Hamiltonian (1) in the canonical ensemble depends crucially on the ratio $d/\Delta = \frac{2}{L}\sinh(1/g)$ between the level spacing d and the bulk superconducting gap Δ [10]. In the weak-coupling regime $d/\Delta \gg 1$, which corresponds to small grains or small coupling constant, there are strong pairing fluctuations above the Fermi sea. In the strong-coupling regime ($d/\Delta \ll 1$), which corresponds to large grains or large coupling constant, superconductivity is fully developed and well described by the grand-canonical BCS theory. These two regimes are connected by a continuous crossover, which exhibits an interesting parity effect, meaning that grains with an odd number of electrons are less superconducting than grains with an even number of electrons.

We shall next describe the entanglement properties of the ground state of (1) with $M = L/2$ pairs of electrons. To do so, it is convenient to recall the standard BCS ansatz of the ground state wave function. The grand-canonical BCS wave function is given by $|\psi_{\rm BCS}\rangle = \exp(P^\dagger)|0\rangle$, where $P^\dagger = \sum_j g_j b_j^\dagger$ is the operator that creates a Cooper pair, with wave function g_j, acting on the Fock vacuum $|0\rangle$. The number of electron pairs in $|\psi_{\rm BCS}\rangle$ is fixed in average through the addition of a chemical potential to the Hamiltonian (1). Ultrasmall superconducting grains have a fixed value of electron pairs $M \sim 10^2$, so the GS is better described by the projected BCS wave function, $|\psi_{\rm PBCS}\rangle \propto (P^\dagger)^M|0\rangle$ [10,15]. The Cooper operator $P^\dagger$ can be split into the sum of the operators below and above the Fermi energy,

$$P^\dagger = P_A^\dagger + P_B^\dagger, \quad P_A^\dagger = \sum_{j=1}^{M} g_j b_j^\dagger, \quad P_B^\dagger = \sum_{j=M+1}^{L} g_j b_j^\dagger, \quad (2)$$

yielding

$$|\psi_{\rm PBCS}\rangle \propto \sum_{n=0}^{M} C_{M,n} (P_A^\dagger)^n |0\rangle_A \otimes (P_B^\dagger)^{M-n}|0\rangle_B, \quad (3)$$

where $C_{M,n} = M!/[n!(M-n)!]$ is a binomial number. If $g = 0$, one has $g_j = 1$ for $j \leqslant M$, and $g_j = 0$ for $j > M$, so (3) coincides with the Fermi state. If $g \to \infty$, one has $g_j = 1, \forall j$, and (3) becomes, upon normalization,

$$\lim_{g\to\infty} |\psi_{\rm PBCS}\rangle = \sum_{n=0}^{M} \psi_n |n\rangle_A \otimes |M-n\rangle_B, \quad (4)$$

where $|n\rangle_A \propto (P_A^\dagger)^n|0\rangle_A$, $|M-n\rangle_B \propto (P_B^\dagger)^{M-n}|0\rangle_B$ are normalized states and

$$\psi_n = \frac{C_{M,n}}{\sqrt{C_{L,M}}}. \quad (5)$$

Equation (4) gives the Schmidt decomposition of the PBCS state corresponding to the partition of the system into the states below the Fermi level (part A) and above the Fermi level (part B). The reduced density matrix for block A can be readily obtained,

$$\rho_A = \sum_{n=0}^{M} \psi_n^2 |n\rangle_A \langle n|_A, \quad (6)$$

so its eigenvalues are $\lambda_n = \psi_n^2$. In the limit where $L \gg 1$ and $n \gg 1$, the highest values of λ_n are concentrated near $n \sim L/4$. The entanglement spectrum (ES), defined as $\epsilon_n = -\ln \lambda_n$, can be approximated by the parabola

$$\epsilon_n \simeq \frac{L}{2}\left(1 - \frac{4n}{L}\right)^2 + \frac{1}{2}\ln\frac{\pi L}{8}, \quad n \sim \frac{L}{4}, \quad (7)$$

so the most probable states are concentrated around $n = L/4$ and deviate an amount of order $\sqrt{L}$. The entanglement entropy of the density matrix (6) is given by

$$S_A = -{\rm Tr}\rho_A \ln \rho_A \simeq \tfrac{1}{2}[\ln(\pi L/8) + 1], \quad (8)$$

and diverges logarithmically with the size of block A. The behavior $\frac{1}{2}\ln L$ is due to the invariance of the GS, at $g \to \infty$, under permutations of all energy levels. A similar logarithmic behavior has been found for ferromagnetic spin chains and the Dicke state at half filling [19,20] (see Ref. [21] for a generalization of this type of states).

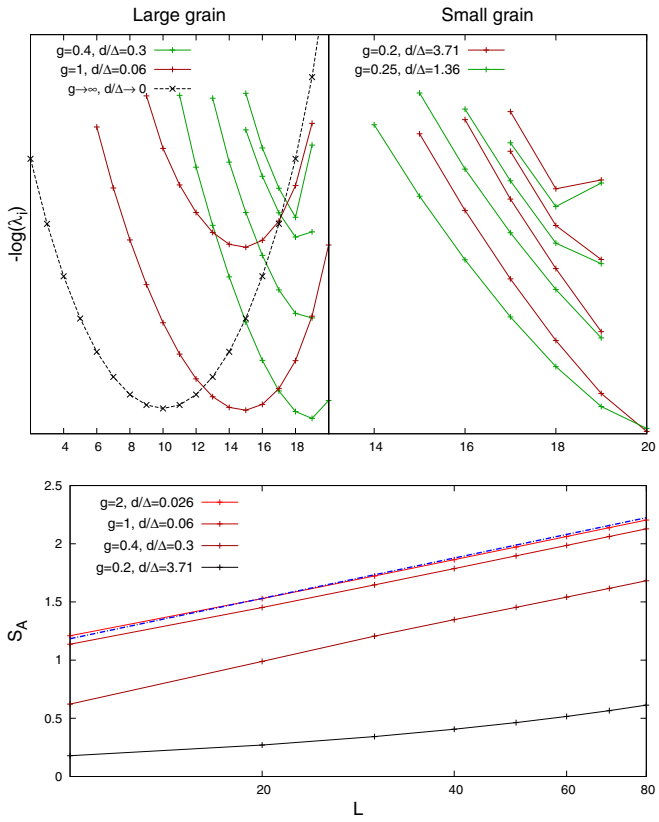

FIG. 1. (Color online) Top: Entanglement spectrum, $\epsilon_i = -\ln\lambda_i$ for the GS of (1) with $L = 40$ and $M = 20$ for the block of levels under the Fermi point. The dotted line corresponds to $g \to \infty$, given approximately in Eq. (7). Bottom: Entanglement entropy for the same block, as a function of the number of levels for different values of g. The dotted line marks the $g \to \infty$ behavior given in Eq. (8).

For moderate values of the BCS coupling constant g, the Schmidt decomposition of the GS of (1) is given by

$$|\Psi_{L,M}\rangle = \sum_{n=0}^{M}\sum_{a=1}^{\chi_n} \psi_{n,a}|n,a\rangle_A \otimes |M-n,a\rangle_B, \quad (9)$$

and involves, in general, χ_n states having n particles in block A (and respectively $M-n$ particles in block B). Note that the PBCS state (4) corresponds to the case $\chi_n = 1, \forall n$. In Fig. 1 (top) we plot the entanglement spectrum $\epsilon_i = -\ln\lambda_i$ of a system with $L = 40$ energy levels, in the three regimes of weak, intermediate, and strong couplings, depending on whether d/Δ is $\gg 1$, $\simeq 1$, or $\ll 1$. Those regimes are linked, respectively, to ultrasmall, small, and large grains. In the weak-coupling case, the most probable state is the Fermi state corresponding to $n = 20$, while the next probable states occur for $n = 19, 18, \ldots$ and are organized approximately into bands with a linear dispersion relation. This structure agrees with the fluctuation-dominated nature of the weak-coupling regime. In the strong-coupling regime one observes the existence of two parabolic bands, corresponding to $\chi_n = 2$. In the limit $g \to \infty$, the higher band disappears and the spectrum is described

by Eq. (7). As g increases, the most probable state, that is, the vertex of the lowest parabola, moves leftwards towards the value $n = L/4$ corresponding to the case $g \to \infty$. The critical value of d/Δ found in the BCS and PBS studies corresponds to the situation where the Fermi state ceases to be the most probable state of the density matrix ρ_A. Concerning the entanglement entropy, we have observed that it behaves as $\frac{1}{2}\ln(L) + \beta$ both in the strong and the intermediate coupling regimes, with β depending on g. As $g \to \infty$, it approaches the expression in Eq. (8), which is marked with the dotted line in Fig. 1. For ultrasmall grains, the logarithmic behavior is lost. In summary, the entanglement spectrum provides a neat picture of the continuous crossover between the weak and strong coupling regimes.

p-wave model. We now turn to the study of the entanglement properties of the 1D p-wave analog of the Richardson model studied in the previous section whose Hamiltonian is given by [13,14]

$$H_p = \sum_{j=1}^{L} d\, j^2\, b_j^\dagger b_j - gd \sum_{j\neq j'}^{L} j\cdot j'\, b_j^\dagger b_{j'}. \qquad (10)$$

The phase diagram of this model can be divided into three regions: weak coupling, $g \leqslant 1/(1-x)$, weak pairing, $1/(1-x) < g \leqslant 1/(1-2x)$, and strong pairing, $g > 1/(1-2x)$, where $x = M/L$ is the filling fraction and M is the number of electron pairs. The weak-pairing and strong-coupling regions are separated by the Read and Green line (RG) $g = 1/(1-2x)$, where the quasiparticle energies are gapless [11]. The corresponding phase transition in 2D is of third order [22], and is characterized by the winding number of the BCS order parameter [11,23]. The weak-pairing phase is topologically nontrivial, and has a Pfaffian wave function similar to the Moore-Read (MR) state of the FQH at filling $\nu = 5/2$. The MR state is the exact GS of (10) on the MR line $g = 1/(1-x)$ and corresponds to a zero-order phase transition meaning that the GS energy is discontinuous when crossing it [13,14]. However, no other discontinuities have been found across the MR line which led to the general belief that the weak-pairing and weak-coupling regions belong in fact to the same phase.

We shall next describe how the different regions of the phase diagram are reflected in the entanglement spectrum and entropy of the ground state. We have considered a system with $L = 40$ energy levels and $M = 10$ pairs, that corresponds to a filling fraction of $x = 1/4$. Figure 2 (top) shows the entanglement energies in the regions: weak coupling ($g = 1$), MR point ($g = 4/3$), weak pairing ($g = 1.5$), RG point ($g = 2$), and strong coupling ($g = 2.5$). As in the s-wave case, the ES forms parabolas whose vertices shift leftwards as g increases, from $n_F = 10$ at $g = 0$ (the Fermi state) to $n = xn_F = 2.5$ as $g \to \infty$, where the levels are equally distributed. At the MR point, i.e., $g = 4/3$, all higher bands of the ES disappear, leaving only one band. This result agrees with the exact GS on the MR line which is a perfect condensate of Cooper pairs [13,14]. Figure 2 (bottom) depicts the total weight of the higher bands as a function of g for a few values of L. It falls to zero at $g = 4/3$ (MR point), as explained above, and presents a local maximum at $g = 2$, the RG point, in accordance with the divergence of the size of the Cooper pairs [22].

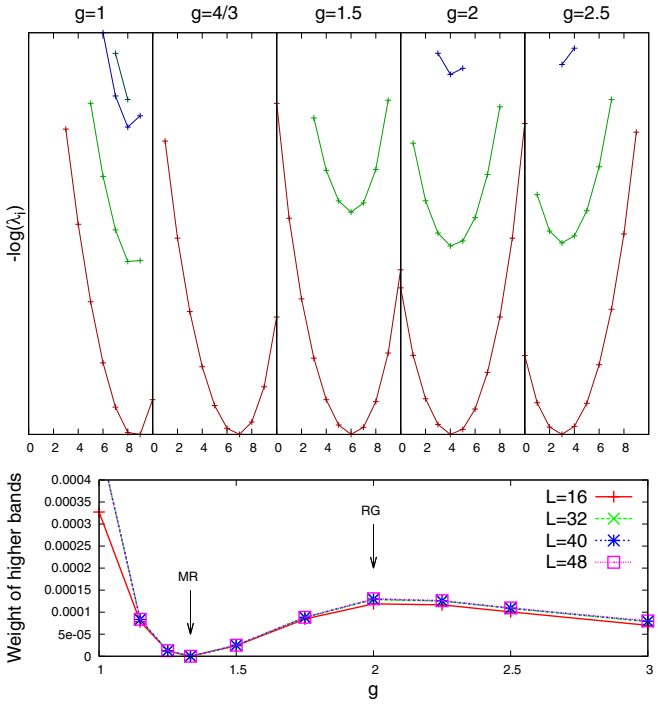

FIG. 2. (Color online) Top: Entanglement spectra of the block A of states below the Fermi level. The abscissas label the number of particles in block A. Bottom: Weight of the higher bands as a function of g, defined as the sum of the density matrix eigenvalues λ_i which do not belong to the lowest band.

Fermi blocks in s wave. The entanglement properties of the BCS models can also be studied using a block $\mathcal{F}(\ell)$ of ℓ levels around the Fermi level n_F; that is, $\mathcal{F}(\ell) = \{n_F - \ell/2 + 1, \ldots, n_F + \ell/2\}$. Only even values of ℓ are allowed until the block reaches one extreme of the energy scale. We shall restrict ourselves to the s-wave Hamiltonian (1) since the p-wave Hamiltonian gives rise to similar results. Let $S_L(\ell, g)$ denote the entanglement entropy associated with block $\mathcal{F}(\ell)$ in the GS of (1) at half filling, $x = \frac{1}{2}$. This quantity is plotted in Fig. 3 for $L = 100$ and several couplings g. For $g \to 0$, the entropy

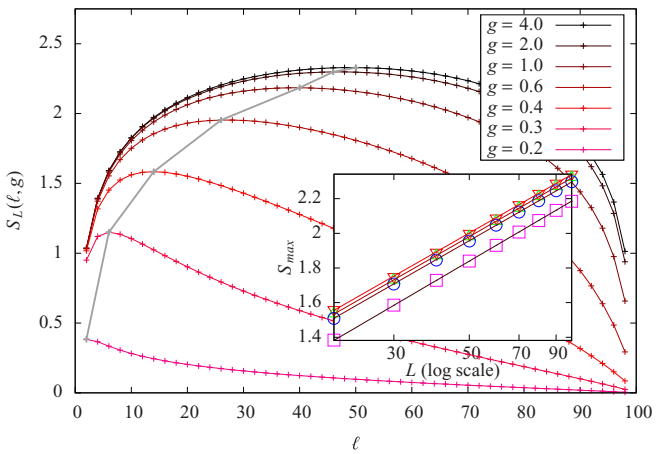

FIG. 3. (Color online) Entanglement entropy $S_L(\ell, g)$, with maxima marked by the polygonal line. Inset: $S_{\max}(L, g)$ for $g = 1$, 2, 3, and ∞, with L in logarithmic scale.

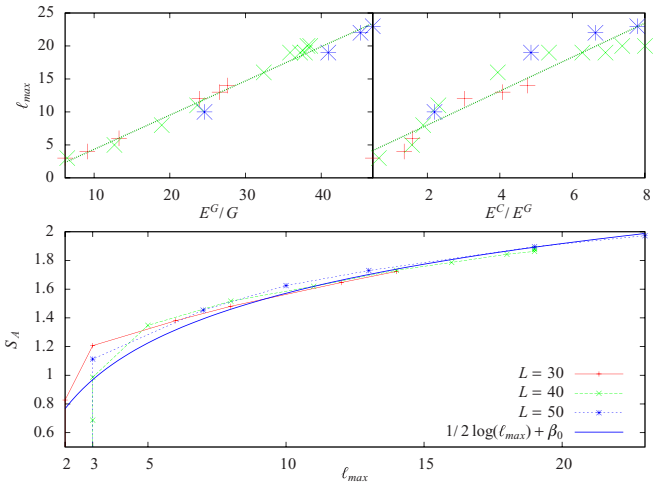

FIG. 4. (Color online) Top left: Correlation between E^G/G and $\ell_{\max}$ in (1); slope is $\frac{1}{2}$. Top right: Correlation between E^C/E^G and $\ell_{\max}$, slope is ≈ 2.5. In both cases, $g \in [0.2,4]$ and $L = 30$, 40, and 50. Bottom: Particle-hole entropy S_A as a function of $\ell_{\max}$, the smooth curve being given by $\frac{1}{2}\ln(\ell_{\max}) + \beta_0$. Notice the collapse of the curves for different values of L.

vanishes, since the GS is the Fermi sea. In the limit $g \to \infty$ the plot becomes symmetric around $\ell = L/2$. As a function of ℓ, $S_L(\ell, g)$ attains a maximum at a value $\ell_{\max}(L, g)$ which depends on L and g, as shown by the polygonal line in Fig. 3. As g increases, this maximum moves from $\ell_{\max} = 1$ to $\ell_{\max} = L/2$ for $g = \infty$. The maximal entropy, $S_{\max}(L, g) \equiv S_L(\ell_{\max}, g)$, is shown in the inset of Fig. 3. For sufficiently large g or L, we have

$$S_{\max}(L, g) \approx \tfrac{1}{2}\ln(L) + \beta(g) + O(L^{-1}), \tag{11}$$

where the coefficient of L^{-1} is $\frac{1}{2}$ for large g. This result is similar to Eq. (8), consistently with the fact that many energy levels are involved at strong coupling. In the p-wave case, we find a similar behavior, but with a different function $\beta(g)$.

In the BCS theory, the number of Cooper pairs is given roughly by the ratio Δ/d, that is, the average number of levels around the Fermi energy involved in pairing correlations [10]. Therefore, one should expect that Δ/d will be related to $\ell_{\max}$, i.e., the size of the Fermi block maximally entangled with the rest of the system. The numerical results show that the relation between these two quantities is given by (see Fig. 4)

$$\ell_{\max} \sim \frac{E^G}{2gd} \overset{\Delta/d \gg 1}{\longrightarrow} \frac{\Delta}{gd} \overset{g \gg 1}{\longrightarrow} \frac{L}{2}, \tag{12}$$

where E^G is the spectroscopic gap. In the canonical ensemble, E^G is the excess of energy required to break a pair of electrons which are subsequently placed at the levels n_F and $n_F + 1$. In the strong-coupling regime, $\Delta/d \gg 1$, the BCS theory gives $E^G = 2\Delta$, that is, the second relation in (12). In the limit $g \gg 1$, the gap behaves as $\Delta \to gdL/2$, which yields $\ell_{\max} \to L/2$. This value coincides with the size of the block A with maximal entropy.

The bottom panel of Fig. 4 shows the entanglement entropy of the block of levels under the Fermi point as a function of $\ell_{\max}$ for different values of L and g. Notice how the values collapse to a single function which, for the intermediate and strong coupling regimes, approaches $\frac{1}{2}\ln(\ell_{\max}) + \beta_0$, with $\beta_0 \approx 0.42$. This collapse supports the conjecture that $2\ell_{\max}$ levels around the Fermi point sustain a BCS state, and account for the entropy of the system; i.e., they constitute the *active levels* of the system. This suggests that keeping $2\ell_{\max}$ states in the DMRG should give an accurate estimate of the low-energy properties of the system. For $\ell_{\max} \simeq 1$, the relation loses meaning, due to the lack of accuracy in the definition of $\ell_{\max}$.

To sum up, we have explored the entanglement of blocks of energy levels in the ground state of pairing Hamiltonians, emphasizing the logarithmic behavior of the maximal entanglement entropy, $\frac{1}{2}\ln(L)$, which is related to the permutation symmetry of the state in the strong-coupling limit. We also showed the relation between the size of the maximally entangled block and the number of active Cooper pairs, which shows up in the spectroscopic gap and the condensation energy. Alongside, we have analyzed the entanglement spectrum and its parabolic band structure, clarifying the nature of the Moore-Read and Read-Green points in the p-wave superconductivity phase diagram in terms of the weight of the lowest band. These results represent a further step towards the characterization of quantum criticality in low-dimensional systems in terms of quantum information quantities.

We would like to stress two lines of future research: (1) to extend our methods to different models of superconductivity (e.g., the Kitaev model [24]) in order to assess the generality of the aforementioned results; (2) to employ the concept of active superconducting levels to the analysis of dynamical and thermal properties in ultrasmall grains.

Acknowledgments. We thank J. Dukelsky, O. Castro-Alvaredo, and B. Doyon for very useful discussions, and acknowledge financial support from Spanish Government Research Project No. FIS2012-33642 and the Severo Ochoa program. J.R.-L. acknowledges also Research Project No. FIS2009-07277, TOQUATA, and ERC grant QUAGATUA.

[1] L. Amico *et al.*, Rev. Mod. Phys. **80**, 517 (2008).

[2] H. Li and F. D. M. Haldane, Phys. Rev. Lett. **101**, 010504 (2008).

[3] P. Calabrese and A. Lefevre, Phys. Rev. A **78**, 032329 (2008); R. Thomale, D. P. Arovas, and B. A. Bernevig, Phys. Rev. Lett. **105**, 116805 (2010); H. Yao and X.-L. Qi, *ibid.* **105**, 080501 (2010); M. Fagotti, P. Calabrese, and J. E. Moore, Phys. Rev. B **83**, 045110 (2011); D. Poilblanc, Phys. Rev. Lett. **105**, 077202 (2010); J. I. Cirac, D. Poilblanc, N. Schuch, and F. Verstraete, Phys. Rev. B **83**, 245134 (2011); X.-L. Qi, H. Katsura, and A. W. W. Ludwig, Phys. Rev. Lett. **108**, 196402 (2012); G. De Chiara, L. Lepori, M. Lewenstein, and A. Sanpera, *ibid.* **109**, 237208 (2012); J. Dubail, N. Read, and E. H. Rezayi, Phys. Rev. B **85**, 115321 (2012); V. Alba, M. Haque, and A. M. Läuchli, Phys. Rev. Lett. **110**, 260403 (2013).

[4] F. Pollmann, A. M. Turner, E. Berg, and M. Oshikawa, Phys. Rev. B **81**, 064439 (2010); A. M. Turner, F. Pollmann, and E. Berg, *ibid.* **83**, 075102 (2011).

[5] M. A. Martin-Delgado, arXiv:quant-ph/0207026.

[6] C. Dunning, J. Links, and H.-Q. Zhou, Phys. Rev. Lett. **94**, 227002 (2005).
[7] V. Balasubramanian, M. B. McDermott, and M. Van Raamsdonk, Phys. Rev. D **86**, 045014 (2012).
[8] T. Xiang, Phys. Rev. B **53**, R10445 (1996).
[9] J. Dukelsky, S. Pittel, and G. Sierra, Rev. Mod. Phys. **76**, 643 (2004).
[10] J. von Delft, Ann. Phys. (Leipzig) **10**, 219 (2001).
[11] N. Read and D. Green, Phys. Rev. B **61**, 10267 (2000).
[12] J. Alicea, Rep. Prog. Phys. **75**, 076501 (2012).
[13] M. Ibáñez, J. Links, G. Sierra, and S.-Y. Zhao, Phys. Rev. B **79**, 180501 (2009).
[14] C. Dunning, M. Ibañez, J. Links, G. Sierra, and S.-Y. Zhao, J. Stat. Mech.: Theory Exp. (2010) P08025.
[15] J. Dukelsky and G. Sierra, Phys. Rev. Lett. **83**, 172 (1999); Phys. Rev. B **61**, 12302 (2000).
[16] N. Bray-Ali, L. Ding, and S. Haas, Phys. Rev. B **80**, 180504(R) (2009).
[17] R. Richardson, Phys. Lett. **3**, 277 (1963); J. Math. Phys. **6**, 1034 (1965).
[18] M. Gaudin, *États propres et valeurs propres de l'Hamiltonian d'appariement* (Les Éditions de Physique, Les Ulis, 1995).
[19] J. K. Stockton, J. M. Geremia, A. C. Doherty, and H. Mabuchi, Phys. Rev. A **67**, 022112 (2003).
[20] V. Popkov and M. Salerno, Phys. Rev. A **71**, 012301 (2005).
[21] O. A. Castro-Alvaredo and B. Doyon, Phys. Rev. Lett. **108**, 120401 (2012); J. Stat. Mech.: Theory Exp. (2013) P02016.
[22] S. M. A. Rombouts, J. Dukelsky, and G. Ortiz, Phys. Rev. B **82**, 224510 (2010).
[23] G. E. Volovik, Zh. Eksp. Teor. Fiz. **94**, 123 (1988) [Sov. Phys. JETP **67**, 1804 (1988)].
[24] A. Y. Kitaev, Phys. Usp. **44**, 131 (2001).